

Periodic orbits of active particles induced by hydrodynamic monopoles

Austen Bolitho,^{1,*} Rajesh Singh,^{1,†} and R. Adhikari^{1,2,‡}

¹*DAMTP, Centre for Mathematical Sciences, University of Cambridge, Cambridge CB3 0WA, United Kingdom*

²*The Institute of Mathematical Sciences-HBNI, CIT Campus, Chennai 600113, India*

Terrestrial experiments on active particles, such as *Volvox*, involve gravitational forces, torques and accompanying monopolar fluid flows. Taking these into account, we analyse the dynamics of a pair of self-propelling, self-spinning active particles confined between parallel planes. Neglecting flow reflected by the planes, the dynamics of orientation and horizontal separation is symplectic, with a Hamiltonian exactly determining limit cycle oscillations. Near the bottom plane, gravitational torque damps and reflected flow excites this oscillator, sustaining a second limit cycle that can be perturbatively related to the first. Our work provides a theory for dancing *Volvox* and highlights the importance of monopolar flow in active matter.

Since Lighthill's seminal work on the squirming motion of a sphere [1, 2], it has been understood that freely moving active particles produce hydrodynamic flows that disallow monopoles and antisymmetric dipoles [3]. The representing of active flows by the symmetric dipole, the leading term consistent with force-free, torque free-motion, has been the basis of much theoretical work in both particle [4–6] and field representations of active matter [7, 8]. The importance of multipoles beyond leading order in representing experimentally measured flows around active particles has now been recognized and their effects have been included in recent theoretical work [9, 10]. Less recognised, however, is the fact that active particles in typical experiments [4, 11–16] are neither force- nor torque-free: mismatches between particle and solvent densities lead to net gravitational forces while mismatches between the gravitational and geometric centers lead to net gravitational torques. Then, both monopolar and antisymmetric dipolar flows are allowed and become dominant, at long distances, over active contributions. It is of great interest, therefore, to understand how these components influence the dynamics of active particles and, more generally, of active matter.

Previous studies of this aspect of active matter are limited. Sedimentation equilibrium of hydrodynamically interacting run-and-tumble particles and their dynamics in harmonic confinement has been investigated using lattice Boltzmann [17] and boundary integral methods [18] and the role of re-orientation by the vorticity of monopolar flow has been identified as the key mechanism in the emergence of the pumping state. Monopolar flows near boundaries have also been identified as the operative mechanism behind flow-induced phase separation [19]. However, none of these studies have focussed on the dynamics of pairs, which forms the foundation for understanding collective motion, or attempted an analytical description of motion.

In this Letter, we provide a theory for the dynamics of density-mismatched, bottom-heavy, self-propelling and self-spinning active particles confined between parallel planes. Starting from the ten-dimensional equations for hydrodynamically interacting active motion in the pres-

ence of forces and torques, we derive, by exploiting symmetries, a lower-dimensional dynamical system for the pair. For positive buoyant mass, negative gravitaxis, and negligible reflected flow, we obtain a sedimenting state with limit cycle oscillations in the relative orientation and horizontal separation. The dynamics is symplectic and a Hamiltonian completely determines the properties of periodic orbits. On approach to the bottom wall, reflected flow arrests sedimentation and yields a levitating state with limit cycle oscillations that now includes the mean height. This second limit cycle can be understood as a damped (by gravitational torque) and driven (by reflected flow) perturbation of the first. These rationalise the *Volvox* dance [11, 12] and highlight the importance of monopolar hydrodynamic flow in active matter. We now explain how our results are obtained.

Full and reduced equations: We consider a pair of spherical active particles of radius b , density ρ , self-propulsion speed v_A , and self-rotation speed ω_A , in an incompressible Newtonian fluid of density ρ_f and viscosity η confined between parallel planes whose separation is $L \gg b$. Their geometric centres, propulsive orientations, velocities, and angular velocities are, respectively, \mathbf{R}_i , \mathbf{p}_i , \mathbf{V}_i and $\mathbf{\Omega}_i$, where $i = 1, 2$ is the particle index. Overdamped, hydrodynamically interacting, active motion in the presence of body forces \mathbf{F}_j^B and body torques \mathbf{T}_j^B is given by [20]

$$\mathbf{V}_i = \boldsymbol{\mu}_{ij}^{TT} \cdot \mathbf{F}_j^B + \boldsymbol{\mu}_{ij}^{TR} \cdot \mathbf{T}_j^B + v_A \mathbf{p}_i, \quad (1a)$$

$$\mathbf{\Omega}_i = \boldsymbol{\mu}_{ij}^{RT} \cdot \mathbf{F}_j^B + \boldsymbol{\mu}_{ij}^{RR} \cdot \mathbf{T}_j^B + \omega_A \mathbf{p}_i \quad (1b)$$

where $\boldsymbol{\mu}_{ij}^{\alpha\beta}$ are mobility matrices and repeated particle indices are summed. Positions and orientation obey the kinematic equations $\dot{\mathbf{R}}_i = \mathbf{V}_i$, and $\dot{\mathbf{p}}_i = \mathbf{\Omega}_i \times \mathbf{p}_i$. The above follow directly from Newton's laws for active particles when inertia and active flows are neglected [21]. The expression for the exterior fluid flow $\mathbf{v}(\mathbf{r})$ around the colloids is then: $\mathbf{v}(\mathbf{r}) = (1 + \frac{b^2}{6} \nabla^2) \mathbf{G} \cdot \mathbf{F}_i^B + \frac{1}{2} (\nabla \times \mathbf{G}) \cdot \mathbf{T}_i^B$, where \mathbf{G} is a Green's function of Stokes equation [22] which satisfies the appropriate boundary condition at the boundaries in the flow. For a sphere in a gravitational

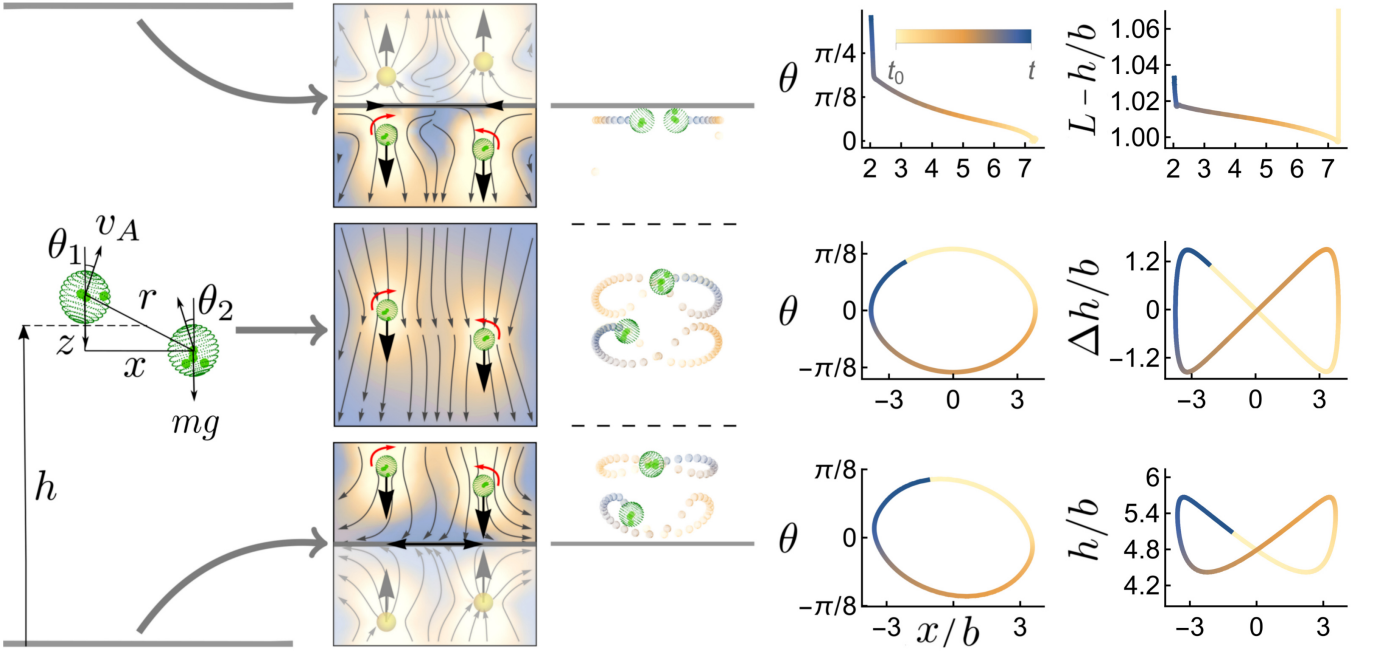


Figure 1. Fixed point and limit cycles of the five-dimensional dynamics system of Eq.(2-3). *First column*: coordinate system used to describe a pair of particles between two parallel plane surfaces. *Second column*: streamlines of the monopolar flow (red curved arrows show flow-induced rotations of the particles) superimposed on a pseudo colormap of the flow speed. The plots in the last four columns correspond to the following three cases: *top row*: near the top surface, *middle row*: away from the surfaces, and *bottom row*: near the bottom surface. *Third column*: stroboscopic images of the two-particle dynamics in the three configurations. The dynamical system admits a fixed point at the top surface, while limit cycles are formed away from the surfaces and near the bottom surface. The last two columns contain the plot of relative orientation θ and average height h as a function of x for the three cases. The colorbar indicates time in last three columns and L is the separation of the planes.

field \mathbf{g} , the force is $\mathbf{F}_i^B = m\mathbf{g}$, where $m = \frac{4\pi b^3}{3}(\rho - \rho_f)$ is the buoyant mass and the torque is $\mathbf{T}_i^B = \mathbf{d}_i \times (\frac{4\pi b^3}{3}\rho\mathbf{g})$, where \mathbf{d}_i is the position of the centre of gravity relative to \mathbf{R}_i [23]. The torque aligns \mathbf{d}_i parallel to \mathbf{g} and positive/negative gravitaxis results when \mathbf{p}_i is parallel/anti-parallel to \mathbf{d}_i . Typical estimates of these parameters for a *Volvox* are $b \sim 300\mu\text{m}$, $v_A \sim 300\mu\text{m/s}$, $mg \sim 1\text{nN}$, $\omega_A \sim 1\text{ rad/s}$ [11]. Thus, the typical active forces $F^A \sim 6\pi\eta b v_A \sim 10^{-9}\text{N}$ and torques $T^A \sim 8\pi\eta b^3 \omega^A \sim 10^{-12}\text{Nm}$. Thus, Brownian forces $k_B T/b \sim 10^{-14}\text{N}$ and torques $k_B T \sim 10^{-20}\text{Nm}$ can be neglected for such systems of active particles. We now present a reduced description of our deterministic equations of motion.

Our dimensional reduction is motivated by a symmetry of Stokes flow that constrains motion initially in a plane perpendicular to the torque to remain in that plane. We choose $y = 0$ to be the plane of motion, set $\mathbf{F}_i^B = -mg\hat{\mathbf{z}}$, $\mathbf{T}_i^B = T_R \mathbf{p}_i \times \hat{\mathbf{z}}$, where $T_R = \frac{4\pi b^3}{3}\rho g d$ is the magnitude of the gravitational torque, and parametrise $\mathbf{R}_i = x_i \hat{\mathbf{x}} + z_i \hat{\mathbf{z}}$ and $\mathbf{p}_i = \sin\theta_i \hat{\mathbf{x}} + \cos\theta_i \hat{\mathbf{z}}$, so that $\mathbf{V}_i = \dot{x}_i \hat{\mathbf{x}} + \dot{z}_i \hat{\mathbf{z}}$, and $\boldsymbol{\Omega}_i = \dot{\theta}_i \hat{\mathbf{y}}$. Using these and translational and time-reversal symmetries in Eq.(1), retaining terms in the mobility matrices to leading order in $x_1 - x_2$, z_1 and z_2 , discarding the decoupled equation for the horizontal com-

ponent of the center of mass, and expressing the result in terms of the reduced variables $2\dot{\psi} = \dot{\theta}_1 + \dot{\theta}_2$, $2\dot{\theta} = \dot{\theta}_1 - \dot{\theta}_2$, $x = x_1 - x_2$, $z = z_1 - z_2$, $2h = z_1 + z_2$, we obtain a five-dimensional dynamical system [21], partitioned into two orientational equations

$$\begin{aligned} \dot{\psi} &= -\frac{T_R}{8\pi\eta b^3} \sin\psi \cos\theta, \\ \dot{\theta} &= -\frac{T_R}{8\pi\eta b^3} \cos\psi \sin\theta - \frac{mg}{8\pi\eta} \left[\frac{x}{r^3} - \frac{x}{(4h^2 + r^2)^{3/2}} \right] \end{aligned} \quad (2)$$

and three positional equations,

$$\begin{aligned} \dot{x} &= 2v_A \cos\psi \sin\theta + \frac{mghx}{2\pi\eta(4h^2 + r^2)^{3/2}}, \\ \dot{z} &= -2v_A \sin\psi \cos\theta - \frac{mgz}{2\pi\eta(4h^2 - z^2)}, \\ \dot{h} &= v_A \cos\psi \cos\theta - \frac{mg}{8\pi\eta} \left(\frac{4}{3b} + \frac{1}{r} + \frac{z^2}{r^3} - \frac{2}{h} \right). \end{aligned} \quad (3)$$

The geometry of the reduced variables is shown in Fig. (1). The orientational equations describe the competition between gravitational torques that restore vertical orientations and hydrodynamic torques, from the vorticity of the monopolar flow, that promotes relative orientation. The first and second positional equations

describe the change in relative separation due to gravitaxis and reflected monopolar flow, the latter of which increases horizontal separation and decreases vertical separation. The third positional equation describes the competition between the tendency of the mean height to increase, due to gravitaxis and reflected monopolar flow, and its tendency to decrease, due to gravitational forces and monopolar flow. These equations describe the sedimentation of a passive pair for $v_A = 0$ [24]. We analyse the balance of these effects, initially neglecting the reflected flow.

Hamiltonian limit cycle: To analyse the sedimenting state, we assume initial heights that are remote from both planes, $0 \ll z_1, z_2 \ll L$ and parameter values, to be identified below, that ensure sedimentation in the mean. The attractor $\psi = 0$ of the first orientational equation, reached on the time scale $\omega_R = T_R/8\pi\eta b^3$, defines the slow manifold $\theta_1 + \theta_2 = 0$. On this slow manifold and neglecting reflected flow, reorientation is principally due to the monopolar vorticity, $\dot{\theta} = -mgx/8\pi\eta r^3$, relative horizontal motion is principally due to gravitaxis, $\dot{x} = 2v_A \sin \theta$, and relative vertical motion is absent, $\dot{z} = 0$. Remarkably, the dynamics has the symplectic form $\dot{x} = -\partial_\theta H$, $\dot{\theta} = \partial_x H$ with Hamiltonian

$$H(x, \theta) = \frac{mg}{8\pi\eta} \frac{1}{\sqrt{x^2 + z^2}} + 2v_A \cos \theta \quad (4)$$

which has the dimension of velocity and is a constant of motion. Position and angle are canonically conjugate variables and the dynamics preserves the two-form $dx \wedge d\theta$. Level sets $H(x, \theta) = E$ of the Hamiltonian, shown in Fig.(2a), define orbits in the $x - \theta$ plane labelled by the “energy” E . For closed orbits, θ vanishes at the turning points and x reaches its maximum x_m , giving $E = mg/8\pi\eta\sqrt{x_m^2 + z^2} + 2v_A \geq 2v_A$ as a bound for such orbits. Trajectories on the orbit are obtained by integrating $dt = -dx/\partial_\theta H = d\theta/\partial_x H$ at constant energy, from which the period follows directly. For small oscillations, a quadratic approximation to the Hamiltonian shows that x and θ vary harmonically with frequency $\omega_0 = 2\pi/T_0 = \sqrt{mgv_A/\eta z^3}$. For large oscillations, the trajectory integrals can be obtained exactly in terms of elliptic functions [25]. The result for the period T_E , scaled by the frequency of small oscillations, is shown in (2b). The mean height is driven by the Hamiltonian limit cycle and its change per period is

$$\frac{\Delta h}{T_E} = -(v_0 + E) + \langle 3v_A \cos \theta - v_0 \frac{3bz^2}{4r^3} \rangle \quad (5)$$

where angled brackets denotes orbital averages at energy E and $v_0 = \frac{mg}{6\pi\eta b}$. The averages on the right can be obtained exactly in terms of elliptic functions and the mean sedimentation speed $\Delta h/T_E$ thus obtained is shown in Fig.(2c). The root of the above equation determines the critical value E_0 of the energy above (below) which

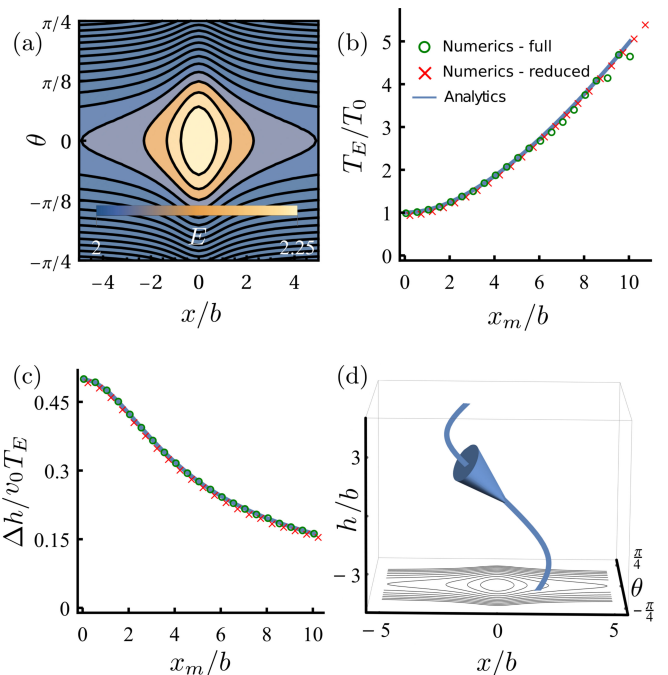


Figure 2. Exact solution of the Hamiltonian limit cycle. (a) levels sets of the Hamiltonian, in which the reflection symmetries $x \rightarrow -x$ and $\theta \rightarrow -\theta$ are clearly visible; (b) variation of the period of large oscillations T_E as a function of their amplitude, scaled by the period of small oscillations; using the experimental values [11], we obtain $T_0 \sim 8s$, giving $T_E \sim 12s$ for $x_m = z = 3$, which is in good agreement with the experimentally measured time period of the “Minuet” bound state [11]. (c) sedimentation speed as a function of the oscillation amplitude; and (d) orbit on a constant energy manifold in x, θ and h with the level sets of H shown on a cross-section. Exact analytical results are compared with numerical simulations of the full and reduced equations in (b) and (c).

the net vertical motion is upward (downward). A typical sedimenting trajectory, $E > E_0$, is shown in $x - \theta - h$ space in Fig.(2c).

The symplectic structure is destroyed when the reorienting effect of the gravitational torque is included, the Hamiltonian increases monotonically at the rate $\dot{H} = TRv_A \sin^2 \theta / 4\pi\eta b^3$ to its maximum value of $mg/8\pi\eta z + 2v_A$ at $x = \theta = 0$, and this corresponds to the pair sedimenting with a vertical separation z and oriented vertically. We next examine how reflected flow alters these exact results.

Limit cycle near bottom plane: The effect of reflected flow appears at different orders of h in the dynamical system. In decreasing order of importance, the height dynamics receives an $O(z/h)$ reduction in the effective mobility, the vertical separation receives an $O(z^2/h^2)$ hydrodynamic attraction, the horizontal separation receives an $O(z^3/h^3)$ hydrodynamic repulsion, and the orientation receives an $O(z^3/h^3)$ contribution to reorientation. A levitating state at a mean height h^* can exist if the

change in the mean height per period is zero, giving

$$-(v_0 + E) + \langle 3v_A \cos \theta - v_0 \left(\frac{3bz^2}{4r^3} - \frac{3b}{2h} \right) \rangle = 0. \quad (6)$$

The rate of change of the Hamiltonian on the true limit cycle is $\dot{H} = T_R v_A \sin^2 \theta / 4\pi\eta b^3 - \left(\frac{mg}{8\pi\eta} \right)^2 \frac{x^2}{2(x^2+z^2)^{3/2}h^2}$ and, if this is to vanish over an orbit, we must have

$$\langle \dot{H} \rangle = \langle 2\omega_R v_A \sin^2 \theta - \frac{9b^2 v_0^2 x^2}{32(x^2+z^2)^{3/2}h^2} \rangle = 0. \quad (7)$$

To $O(z^3/h^3)$ the average over the true limit cycle can be replaced by an average over the Hamiltonian limit cycle at some energy E^* [26]. The above pair of equations, in which averages are taken over Hamiltonian orbits, implicitly determines the values of h^* and E^* for which a levitating, periodic bound-state can exist in the presence of reflected flow. The vertical separation is driven to zero unless there are short-range effects, unaccounted for in the above equations, that provide countervailing effects.

Fixed point at top plane: For energy values $E < E_0$ the net vertical motion is upwards. Then, the dynamical system must be modified to account for the proximity of the top plane. This is obtained by replacing h by $\pm(L-h)$ in Eqs.(2-3). The effect of reflected flow from the top surface is now the opposite and instead of being destabilising is stabilising. The limit cycle is destroyed and, instead, a dimerised state is obtained due to the attractive flow of the monopoles pointing away from the plane. This is identical in mechanism but distinct in detail to flow-induced phase separation of active particles which swim into the plane surface [19].

Conclusion: We have shown the existence of bound states from the interplay of self-propulsion and monopolar hydrodynamic interactions in three dimensions. The increased symmetry of the freely sedimenting 2 body problem yields an analytical solution [27, 28] of curves which foliate the dynamical subspace in a similar way to a simple pendulum.

The monopolar flow near the bottom surface is of similar symmetry as that of a contractile dipole in an unbounded domain, while the flow at the top surface is reminiscent of an extensile dipole, whose axes are along the normal to the surface. This explains planar repulsion at the bottom surface, which when coupled with self-propulsion and reorientations, leads to the formation of a stable limit cycle. The extensile nature of the flow at the top surface explains the fixed point of the dynamical systems. Near the bottom surface a unique stable limit cycle emerges in the same way frictional damping and time dependent forcing produce a unique steady state in oscillators. The monopolar flow required for this mechanism is operative for either a no-shear or a no-slip plane surface. Simulations confirm this result as qualitatively the

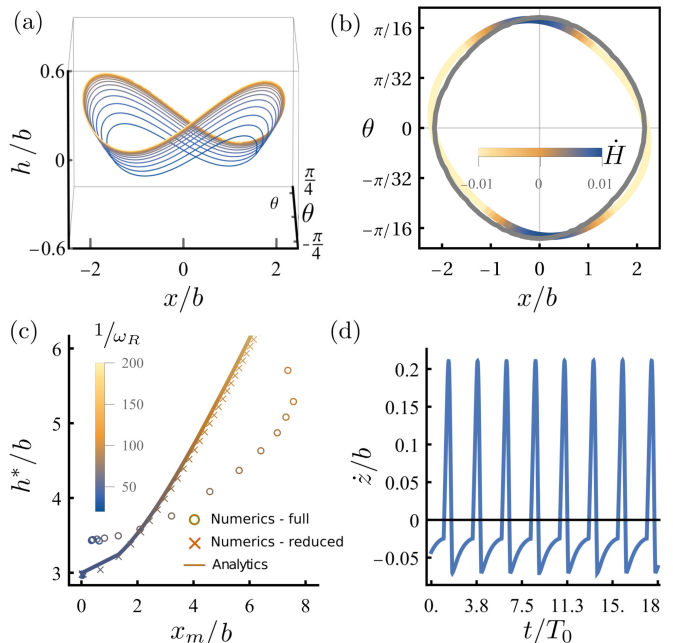


Figure 3. Perturbative solution of the two-body system near the bottom plane; (a) a stable limit cycle is formed in the presence of the bottom plane; (b) an overlay of the numeric and analytic contours with $E = 2.2$. The colormap shows instantaneous “power” input into the numerical limit cycle from perturbative effects which produce small deformations to the shape of the orbit; (c) shows the period averaged levitation height from the bottom plane h^*/z against the maximum amplitude x_m for the limit cycle as ω_R is varied. Excellent agreement is shown between the analytic solution in Eqs.(6-7) and the reduced numerics; and (d) the assumption $\dot{z} = 0$ breaks down near a plane surface when considering the full equations of motion in Eq.(3). This leads to disagreement with the full numerics in (c).

orbits are unchanged when a no-slip surface is used. The time scales of the dynamics at the plane no-slip surface is longer as the hydrodynamic interactions are weaker when compared with the plane no-shear surface (see sec IV of the SI [21]). A detailed multiparticle description and the roles of higher order multipoles will be presented elsewhere [29].

Acknowledgements: We acknowledge the EPSRC (AB), the Royal Society-SERB Newton International Fellowship (RS) and the Isaac Newton Trust (RA) for support. We thank Profs. M. E. Cates for critical remarks and Prof. R. E. Goldstein for helpful discussions.

* ab2075@cam.ac.uk

† rs2004@cam.ac.uk

‡ ra413@cam.ac.uk, rjoy@imsc.res.in

[1] M. J. Lighthill, “On the squirming motion of nearly spherical deformable bodies through liquids at very small Reynolds numbers,” *Commun. Pure. Appl. Math.* **5**, 109–

- 118 (1952).
- [2] J. R. Blake, “A spherical envelope approach to ciliary propulsion,” *J. Fluid Mech.* **46**, 199–208 (1971).
 - [3] J. L. Anderson, “Colloid transport by interfacial forces,” *Annu. Rev. Fluid Mech.* **21**, 61–99 (1989).
 - [4] K. Drescher, R. E. Goldstein, N. Michel, M. Polin, and I. Tuval, “Direct measurement of the flow field around swimming microorganisms,” *Phys. Rev. Lett.* **105**, 168101 (2010).
 - [5] E. Lauga and T. R. Powers, “The hydrodynamics of swimming microorganisms,” *Rep. Prog. Phys.* **72**, 096601 (2009).
 - [6] D. L. Koch and G. Subramanian, “Collective hydrodynamics of swimming microorganisms: Living fluids,” *Annu. Rev. Fluid Mech.* **43**, 637–659 (2011).
 - [7] M. C. Marchetti, J. F. Joanny, S. Ramaswamy, T. B. Liverpool, J. Prost, Madan Rao, and R. Aditi Simha, “Hydrodynamics of soft active matter,” *Rev. Mod. Phys.* **85**, 1143–1189 (2013).
 - [8] S. Ramaswamy, “Active matter,” *J. Stat. Mech.* **2017**, 054002 (2017).
 - [9] S. Ghose and R. Adhikari, “Irreducible Representations of Oscillatory and Swirling Flows in Active Soft Matter,” *Phys. Rev. Lett.* **112**, 118102 (2014).
 - [10] T. J. Pedley, D. R. Brumley, and R. E. Goldstein, “Squirmlers with swirl: a model for Volvox swimming,” *Journal of Fluid Mechanics* **798**, 165–186 (2016).
 - [11] K. Drescher, K. C. Leptos, I. Tuval, T. Ishikawa, T. J. Pedley, and R. E. Goldstein, “Dancing Volvox: Hydrodynamic bound states of swimming algae,” *Phys. Rev. Lett.* **102**, 168101 (2009).
 - [12] R. E. Goldstein, “Green algae as model organisms for biological fluid dynamics,” *Ann. Rev. Fluid Mech.* **47**, 343–375 (2015).
 - [13] J. Palacci, S. Sacanna, A. P. Steinberg, D. J. Pine, and P. M. Chaikin, “Living crystals of light-activated colloidal surfers,” *Science* **339**, 936–940 (2013).
 - [14] J. Palacci, C. Cottin-Bizonne, C. Ybert, and L. Bocquet, “Sedimentation and Effective Temperature of Active Colloidal Suspensions,” *Phys. Rev. Lett.* **105**, 088304 (2010).
 - [15] I. Buttinoni, J. Bialké, F. Kümmel, H. Löwen, C. Bechinger, and T. Speck, “Dynamical Clustering and Phase Separation in Suspensions of Self-Propelled Colloidal Particles,” *Phys. Rev. Lett.* **110**, 238301 (2013).
 - [16] S. J. Ebbens and J. R. Howse, “In pursuit of propulsion at the nanoscale,” *Soft Matter* **6**, 726–738 (2010).
 - [17] R. W. Nash, R. Adhikari, J. Tailleur, and M. E. Cates, “Run-and-Tumble Particles with Hydrodynamics: Sedimentation, Trapping, and Upstream Swimming,” *Phys. Rev. Lett.* **104**, 258101 (2010).
 - [18] R. Singh, S. Ghose, and R. Adhikari, “Many-body microhydrodynamics of colloidal particles with active boundary layers,” *J. Stat. Mech* **2015**, P06017 (2015).
 - [19] R. Singh and R. Adhikari, “Universal hydrodynamic mechanisms for crystallization in active colloidal suspensions,” *Phys. Rev. Lett.* **117**, 228002 (2016).
 - [20] R. Singh and R. Adhikari, “Generalized Stokes laws for active colloids and their applications,” *J. Phys. Commun.* **2**, 025025 (2018).
 - [21] “See Supplemental Material at [to be inserted] which includes the details of the calculations, simulation details, and movies of dynamics.”
 - [22] C. Pozrikidis, *Boundary Integral and Singularity Methods for Linearized Viscous Flow* (Cambridge University Press, 1992).
 - [23] T. J. Pedley and J. O. Kessler, “Hydrodynamic phenomena in suspensions of swimming microorganisms,” *Annu. Rev. Fluid Mech.* **24**, 313–358 (1992).
 - [24] M. Smoluchowski, “On the mutual action of spheres which move in a viscous liquid,” *Bull. Acad. Sci. Cracovie A* **1**, 28–39 (1911).
 - [25] I.S. Gradshteyn and I.M. Ryzhik, “Table of Integrals, Series, and Products,” (Academic Press, 2014) pp. 63–247.
 - [26] N.M. Krylov and N. N. Bogoliūz ũiŕbov, *Introduction to non-linear mechanics* (Princeton Univ. Press, 1947).
 - [27] B. Cantwell, *Introduction to Symmetry Analysis*, Vol. 29 (Cambridge University Press, 2002).
 - [28] H. Stephani, *Differential equations: their solution using symmetries* (Cambridge University Press, 1989).
 - [29] A. Bolitho *Et. Al.*, “Flow-induced bound states of active particles,” In preparation.
 - [30] A. J. C. Ladd, “Hydrodynamic interactions in a suspension of spherical particles,” *J. Chem. Phys.* **88**, 5051–5063 (1988).
 - [31] R. Singh and R. Adhikari, “Hydrodynamic and phoretic interactions of active particles in Python,” [arXiv:1910.00909](https://arxiv.org/abs/1910.00909) (2019).
 - [32] J. R. Blake, “A note on the image system for a Stokeslet in a no-slip boundary,” *Proc. Camb. Phil. Soc.* **70**, 303–310 (1971).
 - [33] K. Aderogba and J. R. Blake, “Action of a force near the planar surface between semi-infinite immiscible liquids at very low Reynolds numbers,” *Bull. Australian Math. Soc.* **19**, 309–318 (1978).
 - [34] S. Thutupalli, D. Geyer, R. Singh, R. Adhikari, and H. A. Stone, “Flow-induced phase separation of active particles is controlled by boundary conditions,” *Proc. Natl. Acad. Sci.* **115**, 5403–5408 (2018).

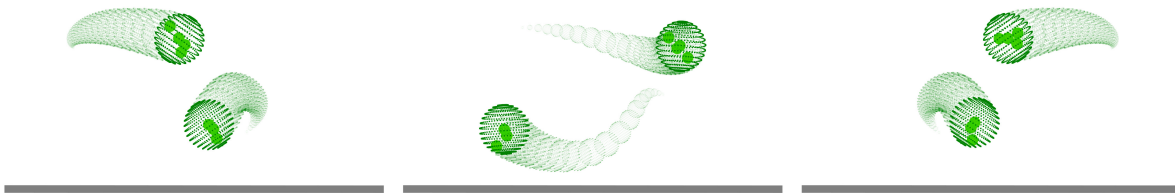


Figure 4. Stroboscopic images from the dynamics of two active particles near a plane no-shear surface. A similar dynamics is also obtained near a plane no-slip surface but with a longer time scale due to reduced strength of the hydrodynamic interactions.

SUPPLEMENTAL INFORMATION (SI)

I. FULL EQUATIONS OF MOTION AND NUMERICAL SOLUTION

We consider a system of active colloids labeled as $i = 1, \dots, N$ of radius b in an incompressible fluid of viscosity η . The centre of mass of the i th colloid is denoted by \mathbf{R}_i , while a unit vector \mathbf{p}_i denotes its orientation. The translational \mathbf{V}_i and rotational velocity $\mathbf{\Omega}_i$ is given from the sum of all the forces and torques acting on the colloids

$$\begin{aligned} m\dot{\mathbf{V}}_i &= -\gamma_{ij}^{TT} \cdot (\mathbf{V}_j - v_A \mathbf{p}_j) - \gamma_{ij}^{TR} \cdot (\mathbf{\Omega}_j - \omega_A \mathbf{p}_j) + \mathbf{F}_i^B = 0 \\ I\dot{\mathbf{\Omega}}_i &= -\gamma_{ij}^{RT} \cdot (\mathbf{V}_j - v_A \mathbf{p}_j) - \gamma_{ij}^{RR} \cdot (\mathbf{\Omega}_j - \omega_A \mathbf{p}_j) + \mathbf{T}_i^B = 0 \end{aligned}$$

Here v_A (and ω_A) is the self-propulsion translational (rotational) speed of an isolated colloid, $\gamma^{\alpha\beta}$, for $(\alpha, \beta = T, R)$, are friction tensors [30], while \mathbf{F}_i^B and \mathbf{T}_i^B are the body forces and torques on the i th colloid.

In the microhydrodynamic regime, as applicable to colloidal scale, the inertia can be ignored, and the rigid body motion is then given as [20, 30]

$$\begin{aligned} \mathbf{V}_i &= \boldsymbol{\mu}_{ij}^{TT} \cdot \mathbf{F}_j^B + \boldsymbol{\mu}_{ij}^{TR} \cdot \mathbf{T}_j^B + v_A \mathbf{p}_i \\ \mathbf{\Omega}_i &= \boldsymbol{\mu}_{ij}^{RT} \cdot \mathbf{F}_j^B + \boldsymbol{\mu}_{ij}^{RR} \cdot \mathbf{T}_j^B + \omega_A \mathbf{p}_i \end{aligned}$$

Here $\boldsymbol{\mu}^{\alpha\beta}$, for $(\alpha, \beta = T, R)$, are the mobility matrices [30].

The above equations have been simulated using PyStokes, a python package for simulating Stokesian hydrodynamics [31]. The initial parameters were set to $b = 1$, $v_A = 1$, $v_0 = 1$. We then study the system near a plane surface by computing the mobility tensors using appropriate an Green's function of Stokes equation which satisfy the boundary conditions of no-slip [32] and no-shear [33] at a plane surface. Our system of active particles near a plane surface has no periodic boundary condition and the particles are allowed to explore the infinite half-space around the surface. For simulations near the bottom plane, an additional restoring torque was added due to bottom-heaviness of the colloids of strength $\omega_R = 0.022$. In this case, z becomes a dynamic variable and the separation changes greatly over the time period of a cycle. In order to prevent the active particles getting too close to one another an additional soft harmonic repulsion of strength 2 was introduced when the particles came within 6.3 units of radius b of one another. This kept the particles separated by an average vertical distance $z = 3$ during integration allowing comparison to be made with the analytics and numerics of the reduced equations. Making this potential soft and longer ranged made numerical integration much more stable while also allowing larger step sizes to be taken, reducing the cost of running longer simulations. It was not necessary to include a repulsive contact potential from the surface as the particles always were at least a distance b away due to hydrodynamic repulsion from the image charges. A two-particle simulation of above equation leads to the formation of time-dependent bound state as described in the main text. See Fig.(4) for snapshots from the dynamics. For simulations near the top surface, the same values were used.

	$\mu_{ij}^{TT} = (1 + \frac{b^2}{3}\nabla^2)\mathbf{G}$	$\mu_{ij}^{TR} = \frac{1}{2}\nabla_{R_j} \times \mathbf{G}$	$\mu_{ij}^{RR} = \frac{1}{4}\nabla_{R_i} \times \nabla_{R_j} \times \mathbf{G}$
Bottom plane	$\mu_{ii}^{zz} = \frac{1}{6\pi\eta b} \left(1 - \frac{3b}{4z_i}\right).$	$\tilde{\mu}_{ii}^{zy} = 0$	$\hat{\mu}_{ii}^{yy} = \frac{1}{8\pi\eta b^3} \left(1 - \frac{1}{16} \frac{b^3}{z_i^3}\right)$
Bottom plane	$\mu_{12}^{xz} = \frac{1}{8\pi\eta} \left[\frac{(x_1-x_2)(z_1-z_2)}{r^3} - \frac{(x_1-x_2)(z_1+z_2)}{r^{*3}} \right]$	$\tilde{\mu}_{12}^{xy} = \frac{1}{8\pi\eta} \left[\frac{(z_1-z_2)}{r^3} - \frac{(z_1+z_2)}{r^{*3}} \right]$	$\hat{\mu}_{12}^{yy} = -\frac{1}{16\pi\eta} \left[\frac{1}{r^3} - \frac{3(y_1-y_2)(y_1-y_2)}{r^5} + \frac{1}{r^{*3}} - \frac{3(y_1-y_2)(y_1-y_2)}{r^{*5}} \right]$
Bottom plane	$\mu_{12}^{zz} = \frac{1}{8\pi\eta} \left[\frac{1}{r} + \frac{(z_1-z_2)(z_1-z_2)}{r^3} - \frac{1}{r^*} - \frac{(z_1+z_2)(z_1+z_2)}{r^{*3}} \right]$	$\tilde{\mu}_{12}^{yz} = \frac{1}{8\pi\eta} \left[\frac{(x_1-x_2)}{r^3} - \frac{(x_1-x_2)}{r^{*3}} \right]$	$\hat{\mu}_{12}^{zy} = -\frac{1}{16\pi\eta} \left[\frac{1}{r^3} + \frac{3(y_1-y_2)(z_1-z_2)}{r^5} - \frac{1}{r^{*3}} - \frac{3(y_1-y_2)(z_1+z_2)}{r^{*5}} \right]$
Top plane	$\mu_{ii}^{zz} = \frac{1}{6\pi\eta b} \left(1 - \frac{3b}{4(L-z_i)}\right).$	$\tilde{\mu}_{ii}^{zy} = 0$	$\hat{\mu}_{ii}^{yy} = \frac{1}{8\pi\eta b^3} \left(1 - \frac{1}{16} \frac{b^3}{(L-z_i)^3}\right)$
Top plane	$\mu_{12}^{xz} = \frac{1}{8\pi\eta} \left[\frac{(x_1-x_2)(z_1-z_2)}{r^3} - \frac{(x_1-x_2)(z_1+z_2-2L)}{r^{*3}} \right]$	$\tilde{\mu}_{12}^{xy} = \frac{1}{8\pi\eta} \left[\frac{(z_1-z_2)}{r^3} - \frac{(z_1+z_2-2L)}{r^{*3}} \right]$	$\hat{\mu}_{12}^{yy} = -\frac{1}{16\pi\eta} \left[\frac{1}{r^3} - \frac{3(y_1-y_2)(y_1-y_2)}{r^5} + \frac{1}{r^{*3}} - \frac{3(y_1-y_2)(y_1-y_2)}{r^{*5}} \right]$
Top plane	$\mu_{12}^{zz} = \frac{1}{8\pi\eta} \left[\frac{1}{r} + \frac{(z_1-z_2)(z_1-z_2)}{r^3} - \frac{1}{r^*} - \frac{(z_1+z_2)(z_1+z_2-2L)}{r^{*3}} \right]$	$\tilde{\mu}_{12}^{yz} = \frac{1}{8\pi\eta} \left[\frac{(x_1-x_2)}{r^3} - \frac{(x_1-x_2)}{r^{*3}} \right]$	$\hat{\mu}_{12}^{zy} = -\frac{1}{16\pi\eta} \left[\frac{1}{r^3} - \frac{3(y_1-y_2)(z_1-z_2)}{r^5} - \frac{1}{r^{*3}} + \frac{3(y_1-y_2)(z_1+z_2-2L)}{r^{*5}} \right]$

Table I. Explicit forms of mobility matrices near the bottom and top parallel no-shear planes, separated by a distance L . The first three rows contain the expression near bottom plane, where the no-shear boundary condition is satisfied. Here $G_{\alpha\beta}(x_1, z_1; x_2, z_2) = G_{\alpha\beta}^o(x_1 - x_2, z_1 - z_2) + (\delta_{\beta\rho}\delta_{\rho\gamma} - \delta_{\beta 3}\delta_{3\gamma})G_{\alpha\gamma}^o(x_1 - x_2, z_1 + z_2)$ is the Green's function of Stokes equation which satisfy the no-shear condition at a plane surface [33], where ρ takes values x, y , which corresponds to directions in the plane surface and $G_{\alpha\beta}^o(\mathbf{r}) = \frac{1}{8\pi\eta} (\nabla^2\delta_{\alpha\beta} - \nabla_\alpha\nabla_\beta)$ r is the Oseen tensor. The vector $r = \sqrt{(x_1 - x_2)^2 + (z_1 - z_2)^2}$ and $r^* = \sqrt{(x_1 - x_2)^2 + (z_1 + z_2)^2}$ are, respectively, distances between the two colloids and the first colloids with the image of the second colloid. The last three rows are expression near the top surface. We emphasize that we do not include any periodic boundary condition and the particles are allowed to explore the full space between the planes.

II. EXACT SOLUTION FOR HAMILTONIAN LIMIT CYCLE

The two-body dynamics (is described in equations 2 and 3 of the main text. In an unbounded domain, it gets simplified to the form

$$\frac{d\theta}{mgx/8\pi\eta r^3} = \frac{dx}{2v_A \sin\theta} = \frac{dh}{v_A \cos\theta - \frac{mg}{8\pi\eta} \left(\frac{4}{3b} + \frac{1}{r} + \frac{z^2}{r^3} \right)} = dt.$$

All the remaining variables are not dynamical. In particular, the separation z between the particles now remains constant. In this limit, we obtain a 1st integral

$$H(x, \theta) = \frac{mg}{8\pi\eta} \frac{1}{\sqrt{x^2 + z^2}} + 2v_A \cos\theta. \quad (9)$$

We denote the level sets as $H(x, \theta) = E$. We now use fact that z is a constant and perform following substitutions

$$x = z \tan\phi, \quad mg = 6\pi\eta b v_0. \quad (10)$$

We can then find the time integrals $\int^t O dt'$ for any quantity $O(\phi(t), E)$ that can be expressed in the form $c_0 + c_1 \cos\phi + c_2 \cos^2\phi + c_3 \cos^3\phi$. Throughout, we use the variable substitution $\int^{T_E} O dt = \int^{x_m} \frac{O}{\dot{x}} dx = \int^{\phi_x} \frac{O}{\dot{\phi}} d\phi$, where $x_m = z \tan\phi_m$ and x_m is the maximum amplitude such that $E = \frac{mg}{8\pi\eta} \frac{1}{\sqrt{x_m^2 + z^2}} + 2v_A$. Under these substitutions the integrals of interest take the form

$$\int^{\phi} \frac{c_0 + c_1 \cos\phi' + c_2 \cos^2\phi' + c_3 \cos^3\phi'}{\cos^2\phi' \sqrt{(a_1 - \cos\phi')(\cos\phi' - a_2)}} d\phi. \quad (11)$$

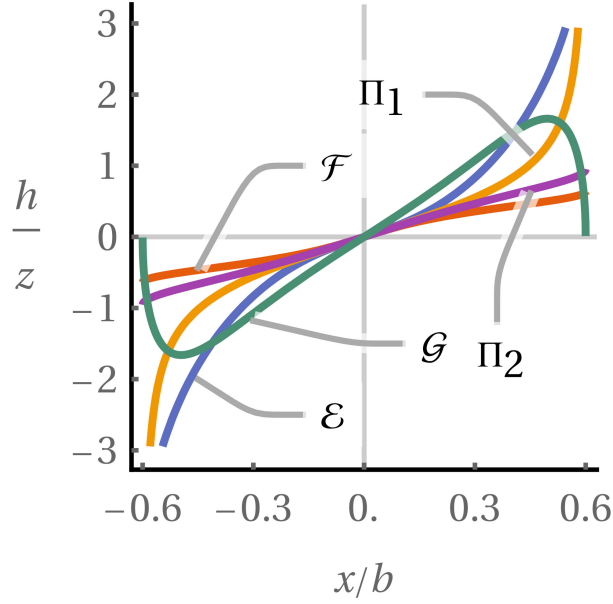


Figure 5. Plots of the 5 basis functions defined in Table (II) for $E = 2.245$.

We can then find an exact solution as a linear combination $\alpha\mathcal{F} + \beta\mathcal{E} + \gamma\Pi_1 + \delta\Pi_2 + \epsilon\mathcal{G}$ of elliptic integrals and a 5th basis function \mathcal{G} (see Table (II)). These integrals then become

$$\int \frac{\sum_{i=0}^3 c_i \left(1 - (n \sin u)^2\right)^i \left(1 + (n \sin u)^2\right)^{3-i}}{\left(1 - (n \sin u)^2\right)^2 \left(1 + (n \sin u)^2\right) \sqrt{\left(1 + \left(\frac{n}{m} \sin u\right)^2\right)}} du, \quad (12)$$

where we have used the definitions

$$\tan \frac{\phi}{2} = n \sin u, \quad n = \sqrt{\frac{1-a_2}{1+a_2}}, \quad m = \sqrt{\frac{a_1-1}{a_1+1}}.$$

By comparison with Table (II) it is easy to see a linear combination of the 5 functions will span the space of the integrand in Eq.(12). The coefficients ($\alpha \dots \epsilon$) are given by

$$\alpha = -\frac{c_0}{a_2} - c_1 + c_2 - c_3, \quad \beta = \frac{(a_1-1)(a_2+1)c_0}{2a_1a_2}, \quad \gamma = c_0 \left(\frac{1}{a_1} + \frac{1}{a_2}\right) + 2c_1, \quad \delta = 2c_3, \quad \epsilon = -\frac{(a_1-1)(a_2-1)c_0}{4a_1a_2}$$

To find the height $h(x, E)$ we start from the dynamical systems and transform x using Eq.(10) to get

$$\begin{aligned} h(x, E) &= \int^{\phi} \frac{\frac{E}{2} - v_0 - \frac{9v_0}{8z} \cos \phi' - \frac{3v_0}{4z} \cos^3 \phi'}{\cos^2 \phi' \sqrt{4v_A^2 - \left(E - \frac{3v_0}{4z} \cos \phi'\right)^2}} d\phi' \\ &= \int^{\phi} \frac{\frac{E}{2} - v_0 - \frac{9v_0}{8z} \cos \phi' - \frac{3v_0}{4z} \cos^3 \phi'}{\cos^2 \phi' \sqrt{\left(2v_A - E + \frac{3v_0}{4z} \cos \phi'\right) \left(2v_A + E - \frac{3v_0}{4z} \cos \phi'\right)}} d\phi'. \end{aligned}$$

The above integral is of the form given in Eq.(11), and thus, can be rendered in the analytic form

$$\frac{4z}{3v_0} (\alpha\mathcal{F} + \beta\mathcal{E} + \gamma\Pi_1 + \delta\Pi_2 + \epsilon\mathcal{G}),$$

$$c_0 = \left(\frac{E}{2} - v_0\right), \quad c_1 = -\frac{9v_0}{8z}, \quad c_2 = 0, \quad c_3 = -\frac{3v_0}{4z}, \quad a = \frac{4z}{3v_0} (2v_A + E), \quad b = \frac{4z}{3v_0} (2v_A - E)$$

The constant of integration can be set to 0 w.l.o.g due to translational invariance in the z direction in the unbounded domain. We can also calculate other useful quantities such as the average sedimentation velocity, the time period of the oscillation and the maximum h amplitude of the closed orbits seen in a co-sedimenting frame of reference

$$\begin{aligned}\langle \dot{h} \rangle &= \frac{1}{T_E} 4 \int_0^{\phi_m} \frac{\dot{h}}{\dot{\phi}} d\phi = 4h(\phi_m, E) \\ T_E &= 4 \int_0^{\phi_m} \frac{d\phi}{\dot{\phi}} = 4 \int_0^{\phi_m} \frac{d\phi}{\sqrt{(2v_A - E + \frac{3v_0}{4z} \cos \phi)(2v_A + E - \frac{3v_0}{4z} \cos \phi) \cos^2 \phi}} \\ \Delta h &= h(\phi_0, E) - \int_0^{\phi_0} \langle \dot{h} \rangle \frac{d\phi}{\dot{\phi}}\end{aligned}$$

where ϕ_0 is the solution of $\frac{E}{2} - v_0 - \frac{9v_0}{8z} \cos \phi_0 - \frac{3v_0}{4z} \cos^3 \phi_0 = 0$. In each case the coefficients for the c_i s can be written down and hence the integral evaluated using Table (II).

	Function	Derivative	Common denominator
\mathcal{F}	$\mathcal{F}\left(u, -\frac{n^2}{m^2}\right)$	$\frac{1}{\sqrt{1 + \frac{n^2}{m^2} \sin^2(u)}}$	$\frac{(1-n^2 \sin^2 u)^2 (1+n^2 \sin^2 u)}{(1-n^2 \sin^2 u)^2 (1+n^2 \sin^2 u) \sqrt{1 + \frac{n^2}{m^2} \sin^2(u)}}$
\mathcal{E}	$\mathcal{E}\left(u, -\frac{n^2}{m^2}\right)$	$\sqrt{1 + \frac{n^2}{m^2} \sin^2(u)}$	$\frac{(1-n^2 \sin^2 u)^2 (1+n^2 \sin^2 u) \left(1 + \frac{n^2}{m^2} \sin^2 u\right)}{(1-n^2 \sin^2 u)^2 (1+n^2 \sin^2 u) \sqrt{1 + \frac{n^2}{m^2} \sin^2 u}}$
Π_1	$\Pi\left(n^2; u, -\frac{n^2}{m^2}\right)$	$\frac{1}{(1-n^2 \sin^2(u)) \sqrt{1 + \frac{n^2}{m^2} \sin^2(u)}}$	$\frac{(1-n^2 \sin^2 u)(1+n^2 \sin^2 u)}{(1-n^2 \sin^2 u)^2 (1+n^2 \sin^2 u) \sqrt{1 + \frac{n^2}{m^2} \sin^2 u}}$
Π_2	$\Pi\left(-n^2; u, -\frac{n^2}{m^2}\right)$	$\frac{1}{(1+n^2 \sin^2(u)) \sqrt{1 + \frac{n^2}{m^2} \sin^2(u)}}$	$\frac{(1-n^2 \sin^2 u)^2}{(1-n^2 \sin^2 u)^2 (1+n^2 \sin^2 u) \sqrt{1 + \frac{n^2}{m^2} \sin^2 u}}$
\mathcal{G}	$\frac{\sin 2u \sqrt{1 + \frac{n^2}{m^2} \sin^2 u}}{1-n^2 \sin^2 u}$	$\frac{2-2\left(2-n^2+2\frac{n^2}{m^2}\right) \sin^2 u + 6\frac{n^2}{m^2} \sin^4 u - 2n^2 \sin^6 u}{(1-n^2 \sin^2 u)^2 \sqrt{1 + \frac{n^2}{m^2} \sin^2 u}}$	$\frac{(1+n^2 \sin^2 u) \left(2-2\left(2-n^2+2\frac{n^2}{m^2}\right) \sin^2 u + 6\frac{n^2}{m^2} \sin^4 u - 2n^2 \sin^6 u\right)}{(1-n^2 \sin^2 u)^2 (1+n^2 \sin^2 u) \sqrt{1 + \frac{n^2}{m^2} \sin^2 u}}$

Table II. The 5 basis functions that make up integral in Eq.(11). $\mathcal{F}, \mathcal{E}, \Pi$ are incomplete elliptic integrals of the first, second and third kind respectively. These have been plotted in Fig.(5).

III. KRYLOV-BOGOLYUBOV AVERAGING OF LIMIT CYCLE AT BOTTOM PLANE

The constant of the motion

$$H(x, \theta) = \frac{mg}{8\pi\eta} \frac{1}{\sqrt{x^2 + z^2}} + 2v_A \cos \theta$$

remains a constant if, to first order, perturbations introduced into the equations of motion cancel. Then the perturbations have no effect on the average orbital quantities. Our equations of motion are

$$\begin{aligned}\dot{\theta} &= -\frac{mgx}{8\pi\eta r^3} - \omega_R \sin \theta \\ \dot{x} &= 2v_A \sin \theta + \frac{9b^2 v_0^2 x}{32h^2},\end{aligned}$$

where the first term on the left hand side is the transient and the second term is the perturbation. The average change of the H over a cycle is given by

$$\langle \dot{H} \rangle = \int^{T_E} \frac{dH}{dt} dt = \int^{T_E} \nabla H \cdot \dot{x} dt \quad (13)$$

$$= \int^{T_E} \nabla H \cdot \Delta dt = \oint \frac{\nabla H \cdot \Delta}{\dot{x}} dx \quad (14)$$

where the transient parts of $\nabla H \cdot \dot{\mathbf{x}}$, which are the equations of motion far from the planes, vanish by the symplectic structure. The remaining part needs to be evaluated for the perturbation vector

$$\Delta = \begin{pmatrix} -\omega_R \sin \theta \\ \frac{9b^2 v_0^2 x}{32h^2} \end{pmatrix}.$$

We require the period average of $\nabla H \cdot \Delta / \dot{\mathbf{x}}$ to vanish to ensure that the average ‘‘energy’’ E^* over a cycle remains constant. We define h^* to be the period averaged height from the bottom plane. This immediately gives the condition

$$\begin{aligned} \langle \dot{H} \rangle &= \left\langle 2\omega_R v_A \sin^2 \theta - \frac{9b^2 v_0^2 x^2}{32(x^2 + z^2)^{3/2} h^{*2}} \right\rangle \\ &= \frac{4}{T_E} \int_0^{x_m} \omega_R \frac{\left[4v_A^2 - \left(E^* - \frac{3bv_0}{4\sqrt{x^2+z^2}} \right)^2 \right] - \frac{9b^2 v_0^2 x^2}{32(x^2+z^2)^{3/2} h^{*2}}}{\sqrt{4v_A^2 - \left(E^* - \frac{3bv_0}{4\sqrt{x^2+z^2}} \right)^2}} dx \\ &= 0 \end{aligned}$$

which, under the transformation $x = z \tan \phi$, gives an integral of the form given in Section II. This condition relates the ‘‘equilibrium’’ height h^* and ‘‘energy’’ E^* . A second condition comes from balancing levitation against sedimentation over a cycle immediately giving

$$\begin{aligned} \langle \dot{h} \rangle &= -(v_0 + E) + \left\langle 3v_A \cos \theta - v_0 \left(\frac{3bz^2}{4r^3} - \frac{3b}{2h^*} \right) \right\rangle. \\ &= -(v_0 + E) + \frac{4}{T_E} \int_0^{x_m} \frac{\frac{3}{2} \left(E^* - \frac{3bv_0}{4\sqrt{x^2+z^2}} \right) - v_0 \left(\frac{3bz^2}{4r^3} - \frac{3b}{2h^*} \right)}{\sqrt{4v_A^2 - \left(E^* - \frac{3bv_0}{4\sqrt{x^2+z^2}} \right)^2}} dx \\ &= 0. \end{aligned}$$

again this integral can be put in the form of Eq. (11) and thus we arrive at a second condition relating h^* and E^* . These can be solved simultaneously to give a unique estimate for the orbit parameters of the limit cycle near the bottom plane. The pair (E^*, h^*) is plotted as a function of ω_R in Figure (3c) in the main text.

IV. EXCHANGE OF DANCING PARTNERS

In this section, we consider two pairs of active particles near a plane no-slip and no-shear surface. We emphasize that the qualitative features of bound states predicted in the main text do not depend on the no-slip or no-shear nature of the plane surface. Here, we show that the interaction times at the no-shear surface is much longer compared to a no-slip surface [34] and that one of the scattering states involves these interacting pairs exchanging partners.

The monopolar flow around an active colloid near the bottom of a parallel plate geometry is of similar symmetry as that of a contractile dipole, whose axis is along the normal to the bottom surface. This has the effect of repulsion between the bound states. These contractile flows also produce a torque on the particles in other pairs which rotate nearby neighbours towards one another. Active swimming is then able to bring the two bound pairs towards one another. Repulsion dominates when pairs are separated $\gg z$ from each other. On the other hand attraction occurs if the pairs are $\sim z$ separated. After the interaction particles can either leave as bound pairs or single particles. Free particles are able to swim up towards the top surface while bound pairs stabilize near the bottom of the cell and continue their dance indefinitely. If a no-slip surface is used instead, the individual dancing behaviour remains the same however the inter-pair interaction is weakened by the no-slip condition. The result is that the timescale for pairs to come into contact is dramatically increased. Otherwise the actual interaction and final states appear qualitatively unchanged (see Figure (6)). We postpone further discussion of this effect to future work. Multiparticle simulations were done with $\omega_R = 0.02$, $v_0 = 0.3$, $v_A = 0.3$. The sedimentation force was reduced in these simulations for integrator stability since the effective hydrodynamic forces on particles becomes extremely large when multiple particles come into close proximity.

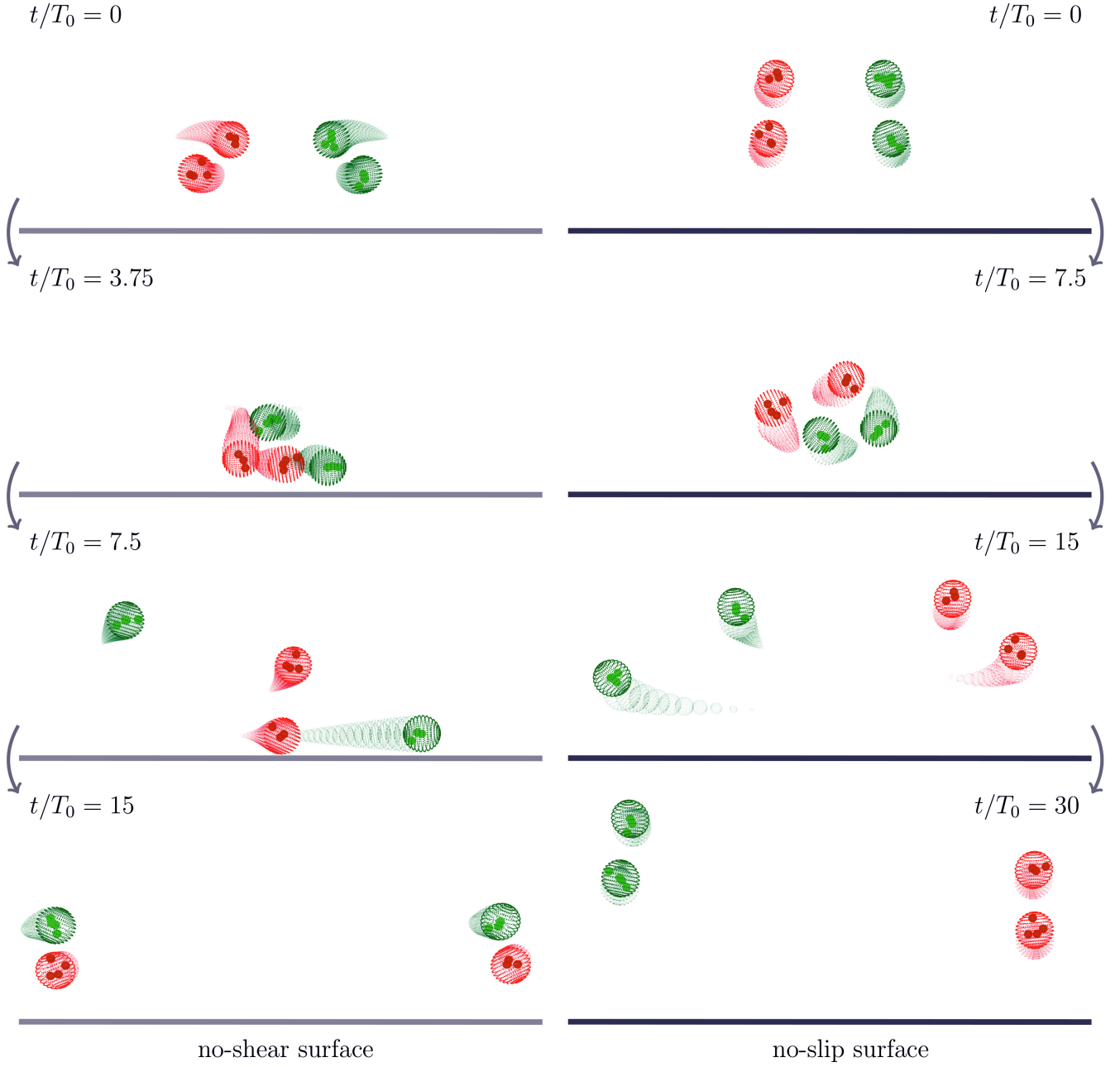


Figure 6. Stroboscopic images of two active bound pairs near a plane no-shear and no-slip surface. The presence of the no-slip condition at the surface weakens hydrodynamic interactions and hence increases the interaction time scale. The particles are pulled down towards the lower surface under the effect of their mutual sedimentation force. Here scattering leads to an exchange of partners in the no-shear geometry and an exchange of places in the no-slip geometry. The end product of scattering events is highly dependent on the initial conditions.